Pre-print submitted version

Dual-source vacuum deposition of pure and mixed halide 2D perovskites: thin film characterization and processing guidelines.

Maria-Grazia La-Placa,[a] Dengyang Guo,[b] Lidón Gil-Escrig,[c] Francisco Palazon,[a] Michele Sessolo,*[a] Henk J. Bolink[a]

[a] *Instituto de Ciencia Molecular, Universidad de Valencia, C/ Beltrán 2, Paterna, 46980, Spain. E-mail: michele.sessolo@uv.es*

[b] *Department of Chemical Engineering, Delft University of Technology, Delft, 2629 HZ, The Netherlands*

[c] *Helmholtz-Zentrum Berlin für Materialien und Energie GmbH, Young Investigator Group for Perovskite Tandem Solar Cells, Kekuléstraße 5, Berlin, 12489, Germany*

The dual-source vacuum deposition of 2D perovskite films of the type PEA_2PbX_4, (PEA = phenetylammonium and X = I^-, Br^-, or a combination of both) is presented. Low-temperature deposited 2D perovskite films showed high crystallinity with the expected trend of bandgap as a function of halide type and concentration. Importantly, we observed an unavoidable halide cross-contamination among different deposition runs, as well as a strong dependence of the material quality with the type of halide precursors used. These findings should be taken into account in the development of vacuum processing for low-dimensional mixed halide perovskites.

Two-dimensional (2D), layered perovskites are a wide family of semiconductors with general formula $(R\text{-}NH_3)_2MX_4$, where inorganic sheets of corner-sharing metal (M, mostly Pb^{2+} and Sn^{2+}) halide (X) octahedra are separated by bilayers of aliphatic or aromatic mono-ammonium cations ($R\text{-}NH_3$), or single layers of diammonium cations.[1,2] 2D perovskites present a large compositional flexibility which allows to design and modulate their electrical and optical properties for specific applications. A wide spectrum of materials can be obtained through simple substitution of halide

anion and organic cations.[3] As in the analogous 3D perovskites,[4] halide substitution/mixing results in marked changes of the optical properties, as the valence band is formed from a mixture of metal s-orbitals and halide p-orbitals, while the conduction band is composed mainly of metal p-orbitals. Increasing the halide electronegativity (from I to Br and Cl) result in a significant downward shift of the valence band maximum and, to a less extent, in an upward shift of the conduction band minimum, thereby increasing the bandgap (E_g).[5,6] In low dimensional perovskites, due to the alternation of inorganic semiconducting and organic insulating sheets, electrons and the holes are confined within the inorganic framework, causing quantum and dielectric confinement effects.[7] These leads to a much higher exciton binding energy (E_b) in 2D perovskites (hundreds of meV) compared to the 3D counterparts (tens of meV).[8,9] In contrast to 3D perovskites, 2D perovskites offers also less restrictions to the size of the cations that can be accommodated between the inorganic sheets, in compliance with the Goldschmidt tolerance parameter.[10,11] While the length of the organic cation has only minor effect on the electronic and optical properties of the semiconductor, its dielectric constant ε_{org}, (which varies depending on the chemical structure of the cation) can be used as a tool to influence E_g and E_b.[9,12,13] The high E_b limits the conversion of excitons to free carriers and consequently the charge carrier mobility in pure 2D perovskites. The latter can be recovered by increasing the thickness of the inorganic slabs such as in 2D Ruddlesden–Popper perovskites.[14] Thanks to the possibility to modulate the optical and electronic properties, 2D perovskites have been investigated for several applications, such as electroluminescence device (LED),[15,16] field effect transistors (FET),[17] photodetector[18,19] and solar cells.[20–22] 2D perovskites were initially studied in the 1990s and recently the interest towards this family of semiconductors is resurgent. While solution processing and single crystal fabrication of 2D hybrid perovskite has been widely reported, vacuum processing of these materials remains rather unexplored. To the best of our knowledge, only one reports exists on fully co-evaporated 2D perovskites,[23] while other works have described a sequential vacuum-deposition and a flash evaporation of low-dimensional Ruddlesden–Popper perovskite films.[11,24–26] Vacuum deposition present important advantages over solution-based methods, such as the fine control over the film thickness, high material purity, and is intrinsically additive. Moreover it eliminate the issues related to the use of solvents such as the solubility limit of the precursors and the presence of resilient solvent in the final film.[27]

In this work we report the synthesis of different pure and mixed halide 2D perovskites by dual source vacuum deposition and we investigated their structural, optical and charge transport properties. We deposited the pure phenethylammonium lead iodide $(PEA)_2PbI_4$ and phenethylammonium lead bromide $(PEA)_2PbBr_4$ by sublimation of the corresponding organic ammonium and metal halides, phenethylammonium iodide (PEAI), phenethylammonium bromide (PEABr), lead iodide (PbI_2) and lead bromide ($PbBr_2$). Furthermore, we explore the preparation of mixed halide compounds using different organic and lead halide precursors. In particular, we co-deposited perovskite films using PEABr and PbI_2 or PEAI and $PbBr_2$, respectively. The 2D films were deposited by simultaneous co-deposition of the precursors, after the calibration of the deposition rate of each compound. The calibration factors were obtained by comparing the thickness of the thin-films as detected from the quartz crystal microbalance sensors with that measured with a mechanical profilometer. Organic salts are often not thermally stable and not easy to sublime due to the possible dissociation in their volatile precursors.[28] However, once properly outgassed in a high vacuum chamber, PEAI and PEABr can be sublimed with a low and stable rate at the minimum temperature required for evaporation, around 160 °C. The inorganic materials were sublimed at temperatures ranging from 260 to 300 °C.

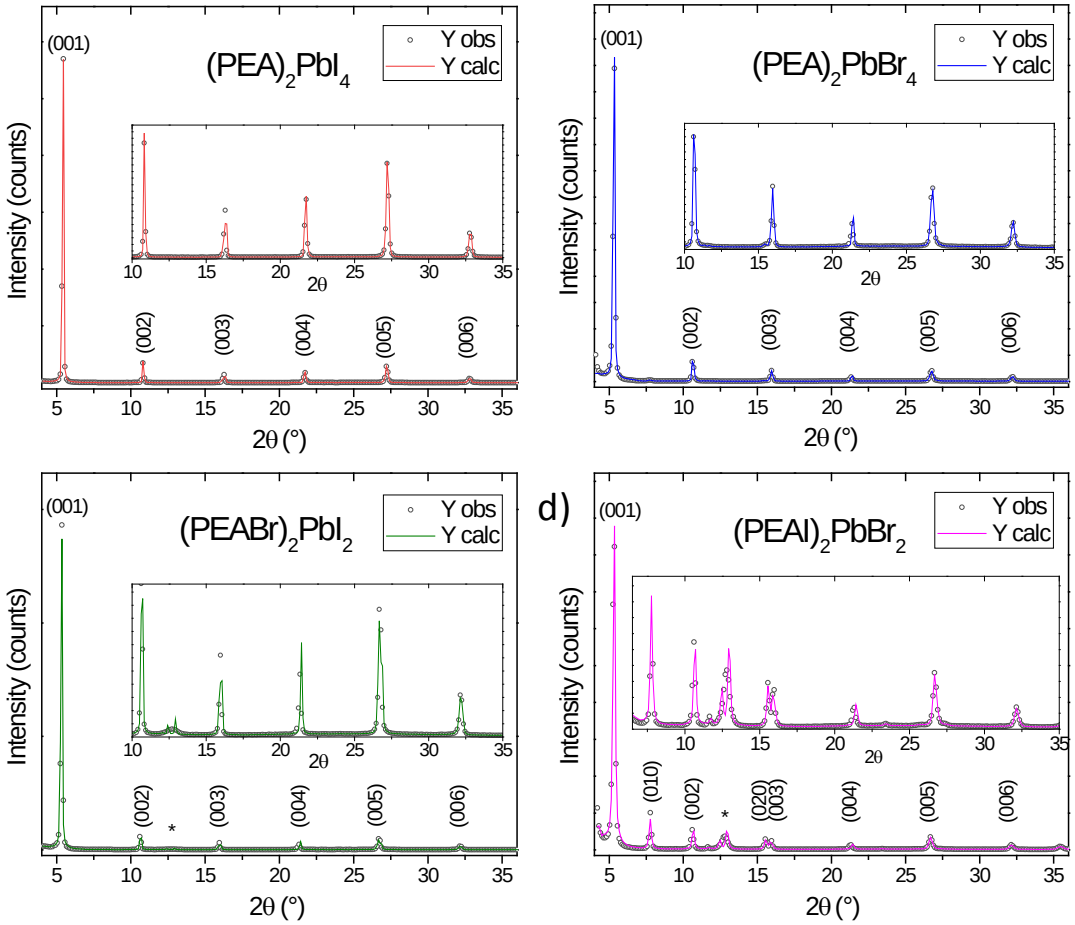

Fig. 1 X-ray diffraction analysis of 200-nm thick, vacuum-deposited 2D perovskites thin films after annealing for 5 min at 100 °C. "Y obs" indicates the experimental traces while "Y calc" indicates the calculated intensities based on whole-pattern fitting (Le Bail refinement).

The mixed halide $(PEA)_2PbBr_2I_2$ perovskites films were prepared with the same procedure and will be described in the text as $(PEABr)_2PbI_2$ when deposited by co-sublimation of PEABr and PbI_2 and as $(PEAI)_2PbBr_2$ in the case of PEAI and $PbBr_2$ co-evaporation. All the thin film depositions were performed in the same vacuum chamber. The relative deposition rate of the organic halides and lead salts was 2:1, accordingly with the compounds stoichiometry. Details of the thin-film deposition are provided in the Supporting Information.

The structural features of the layered perovskite were studied by X-ray diffraction (XRD) on co-sublimed thin films (Fig. 1 and S1). As can be seen from Fig. S1, vacuum-deposited films of

$(PEA)_2PbX_4$ (X = Br or I) show similar diffractograms before and after thermal annealing, albeit with more intense and sharper diffraction peaks for annealed samples (especially in the bromide case). This suggests that crystallization of the desired materials occurs directly during the deposition process at room temperature, while crystallinity can be slightly enhanced after a short thermal annealing at 100 ºC. Therefore, we performed thermal annealing as standard process for all compositions. Whole-pattern Le Bail refinements (solid lines) were performed on the acquired diffractograms (open circles) with Fullprof software (see experimental section for details). Fig. 1 shows that all diffractograms can be well-fitted by considering a P -1 space group with varying lattice parameters as detailed in Table 1.

Table 1 Lattice parameters derived from Le Bail fits of different samples. Space group = P -1.

Sample	*a* (Å)	*b* (Å)	*c* (Å)	*α* (°)	*β* (°)	*γ* (°)
$(PEA)_2PbI_4$	11.49	11.73	17.14	99.63	105.36	89.85
$(PEA)_2PbBr_4$	11.60	11.63	17.51	99.57	105.55	89.83
$(PEABr)_2PbI_2$	11.60	11.63	17.49	99.61	105.62	89.81
$(PEAI)_2PbBr_2$	11.60	11.56	17.48	99.59	105.67	89.79

Table 1 shows that as the halogen becomes smaller, the c-axis parameter, perpendicular to the inorganic perovskite sheets, increases from 17.14 Å for $(PEA)_2PbI_4$ to 17.51 Å for $(PEA)_2PbBr_4$. Qualitatively, this can be clearly seen by a shift of the corresponding (00l) peaks to lower angles (see comparison in Fig. S2). This behavior, which could be considered counterintuitive, has already been reported on the same and in similar materials, and it has been attributed to a different orientation of the phenethylammonium cations between the inorganic layers.[29,30] When the octahedra contract (due to smaller and more electronegative halides) the alkylic substituents of the organic cations will adopt a higher angle with respect to the surface of the inorganic slabs and result in a larger distance between them. Furthermore, it is obvious from Fig. 1 that all films show a preferential orientation along the [001] direction (i.e., perovskite slabs parallel to the substrate). This is common for 2D perovskites and 2D materials in general, but not favorable for charge transport within a thin film device.[31–34] In the case of the $(PEAI)_2PbBr_2$ sample prepared from co-sublimation of PEAI and $PbBr_2$ we also note intense reflections for (010) and (020) planes at 2θ = 7.8º and 2θ = 15.6º respectively as well as a broad signal around 2θ = 12.8 º which could be

attributed to a combination of (1-11) and (-1-12) planes and possibly PbI_2 formed from co-sublimation. Hence, it appears that this sample shows a more heterogeneous crystallinity.

The morphology of the 2D perovskites films was studied by scanning electron microscopy (SEM, Fig. 2) and atomic force microscopy (AFM, supporting Information Fig. S4). The top-view SEM image of the $(PEA)_2PbI_4$ perovskite (Fig. 2a) show well-defined, randomly distributed platelets formed by multiple grains with size ranging from 200 nm to 400 nm. The surface was found to be rather rough, with a quite high root mean square roughness and average height (Tab. 2 and Fig. S4a). The pure bromide $(PEA)_2PbBr_4$ perovskite films are also characterized by the presence of platelets, this time more compact compared to the iodide counterpart. The grain size is in the range of hundreds nm and the topography is characterized by a reduce R_{RMS} and a z_{AVG} (Tab. 2 and Fig. S4b). The morphology and grain size of the mixed $(PEABr)_2PbI_2$ perovskite films was found to be very similar to the pure bromide 2D films, although with a much flatter topography as described in Tab. 2. Finally, the $(PEAI)_2PbBr_2$ films (Fig. 2d) presents the more heterogeneous morphology, with small platelets and large lamellar aggregates, resulting in a very rough surface, also in this case with high R_{RMS} and z_{AVG} values (Tab 2 and Fig. S4d). The overall high roughness of the vacuum deposited 2D perovskite films might be related with the slow sublimation of the precursors towards the substrate. Due to the highly oriented crystal structure of 2D perovskite and the high reactivity and affinity of the precursors, the grain growth proceeds faster than the nucleation rate, resulting in rough films with large platelets and other out-of-plane structures.

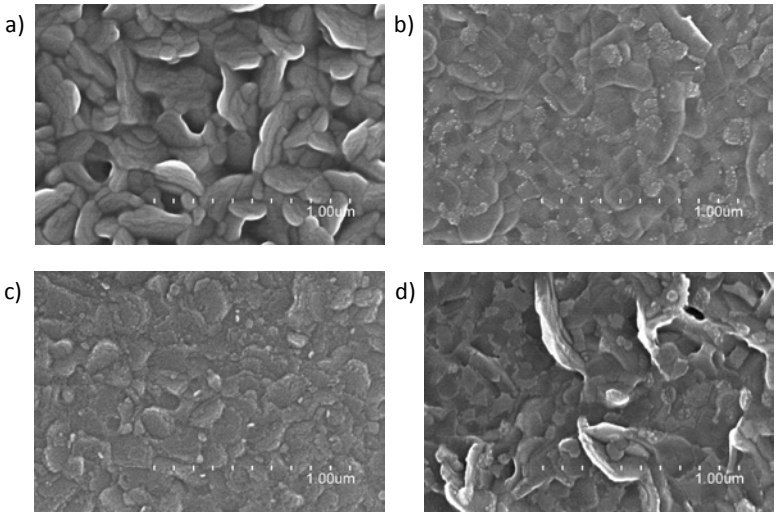

Fig. 2 SEM pictures of vacuum deposited (a) $(PEA)_2PbI_4$ (b) $(PEA)_2PbBr_4$ c) $(PEABr)_2PbI_2$ and d) $(PEAI)_2PbBr_2$ thin-films. The scale bar in all SEM images is 1 µm.

Table 2 Root mean square roughness R_{RMS} and average height z_{AVG} of different samples.

Sample	R_{RMS} (nm)	Z_{AVG} (nm)
$(PEA)_2PbI_4$	25.8	95.0
$(PEA)_2PbBr_4$	10.9	28.3
$(PEABr)_2PbI_2$	4.0	14.1
$(PEAI)_2PbBr_2$	29.2	74.8

The steady state optical characterization of the vacuum-deposited 2D perovskite films is presented in Fig. 3. The optical absorption of the $(PEA)_2PbI_4$ films shows a band in the UV and an intense excitonic peak centered at 503 nm, with a full width at half maximum (FWHM) of 35 nm. When the film of $(PEA)_2PbI_4$ was excited with a LED at 340 nm, intense photoluminescence (yellow dashed line) centered at 521 nm was observed. The peak has a FWHM of 24 nm and a Stokes shift of 80 meV. The values of Stokes shift and FWHM are larger than the ones seen for $(PEA)_2PbI_4$ thin films prepared by solution processing (see supporting information Fig. S3).

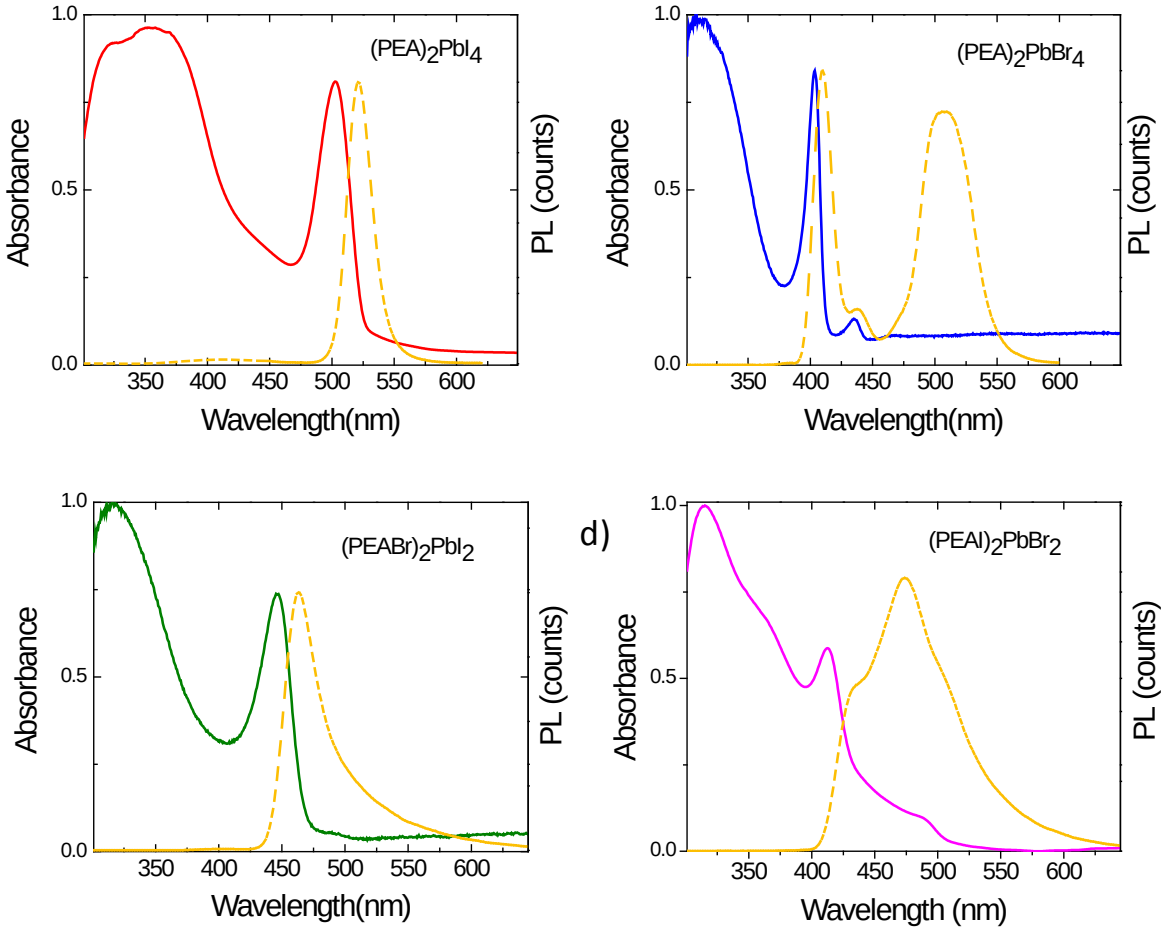

Fig. 3 Optical absorption and photoluminescence spectra (excitation at 340 nm) of 200 nm thick films of (a) $(PEA)_2PbI_4$, (b) $(PEA)_2PbBr_4$, (c) $(PEABr)_2PbI_2$ and (d) $(PEAI)_2PbBr_2$ perovskites.

2D $(PEA)_2PbBr_4$ film exhibit the expected optical absorption band at higher energy, compared to the analogous iodide compound, with a very sharp excitonic peak (FWHM=15 nm) centered at 403 nm. However, another weak absorption band was detected at 434 nm, which cannot be ascribed to the pure PEA_2PbBr_4 phase. Intense and narrow photoluminescence centered at 410 nm and with FWHM of 17 nm was observed, with a small Stokes shift of 60 meV. The excitonic absorption and PL peaks of the vacuum-deposited $(PEA)_2PbBr_4$ 2D perovskite agrees well with the results obtained from solution-processed films, in terms of Stokes shift and FWHM (see supporting information Fig. S3). However, other two peaks were systematically detected in the PL spectrum, a low intensity peak centered at 434 nm and a more intense and broad band centered at 507 nm. Most likely, the additional small intensity peak can be associated to the presence of a

bromide-rich, mixed bromide/iodide phase, while the broad PL band at lower energy can be ascribed to the formation of an iodide-rich phase. This considerations point towards a possible halide cross-contamination in the evaporation chamber, which was used for the vacuum processing of both $(PEA)_2PbBr_4$ and PEA_2PbI_4 perovskite. In order to verify this hypothesis, we carried out energy-dispersive X-ray spectroscopy (EDS) on the films in a scanning electron microscope (SEM). In the 2D $(PEA)_2PbI_4$ films we found an I/Br ratio I/Br = 14.3, indicating that approximately 6% of the total halide content comes from bromide. In the case of the 2D $(PEA)_2PbBr_4$ perovskite, the Br/I ratio was as low as 3.5, meaning that as much as 22% of the total halide content is due to iodide contamination. The EDS analysis justified the observed optical properties of the perovskite film, and clearly indicates that there is cross-contamination between different precursors from different vacuum-deposition runs. Interestingly, in the case of the 2D $(PEA)_2PbI_4$ films there is a rather low bromide contamination, while the contamination of iodide in 2D $(PEA)_2PbBr_4$ films is more relevant. The contamination can be due to i) re-evaporation of previously deposited materials from the surface of the chamber or even to ii) halide exchange between the subliming vapors and the chamber itself. These processes can be more or less pronounced depending on the volatility of the materials as well as on their chemical reactivity, as observed in our iodide and bromide compounds.

The optical absorption of the mixed halide $(PEABr)_2PbI_2$ perovskite (Fig. 3c), deposited by dual source sublimation of PEABr and PbI_2, was found to be blue shifted with respect to that of the $(PEA)_2PbI_4$ and red-shifted compared to $(PEA)_2PbBr_4$, as expected for a mixed halide perovskite. The excitonic absorption was centered at 446 nm (FWHM = 36 nm), while the PL peak was found to be asymmetric with maximum at 464 nm (FWHM= 34 nm), implying a large Stokes shift of 110 meV. The EDS analysis revealed a Br/I ratio of 0.9, very close to the expected stoichiometry for the $(PEABr)_2PbI_2$ perovskite and with only a negligible 2% excess of iodide. At this halide ratio, 3D perovskites usually show halide segregation effects,[35] due to the poor miscibility of the iodide and bromide phases. For this reason, we studied the evolution of the PL over time under continuous laser irradiation (375 nm). Immediately after illumination, we noted the presence of the previously observed high energy peak at 464 nm with a weak component at lower energy (approximately 500 nm). With continuous irradiation, the low energy component dominates the PL spectrum, implying the formation of iodide-rich phases where carriers are efficiently

transferred and radiatively recombine. This is hence in agreement with what generally observed for other mixed halide perovskites.

Rather different optical properties were observed for the other mixed halide $(PEAI)_2PbBr_2$ perovskite films, obtained by simultaneous sublimation of PEAI and $PbBr_2$. The absorption spectrum in Fig. 2d show an excitonic peak at 412 nm, close to that of the pure bromide compounds $(PEA)_2PbBr_4$, and a weak absorption at approximately 490 nm, which is close to the excitonic absorption of the pure iodide $(PEA)_2PbI_4$ perovskite. This behavior suggests the coexistence of different domains, as also confirmed by the PL spectrum, which shows a broad band composed of several peaks: one with maximum at approximately 434 nm and a second, more intense at 475 nm with a shoulder around 504 nm. The optical characteristics are consistent with the presence of a dominant, bromide-rich phase and of a second iodide-rich one. This hypothesis is supported by the elemental analysis, which revealed a Br/I ratio of 1.8, implying that approximately 65% of the halide consists in bromide. The high bromide content of the $(PEAI)_2PbBr_2$ films could also partially explain why the corresponding unit cell parameters are close to those of the $(PEA)_2PbBr_4$ (Table 1). When $PbBr_2$ is reacting with PEAI during the co-deposition process, the halide exchange is limited to an iodide inclusion of about only 30-40 mol%. On the other hand, the co-deposition of PbI_2 and PEABr was found to lead to perovskites with a well-balanced halide content. This phenomenon could be ascribed either to a higher chemical reactivity of PEABr, or to a higher stability of $PbBr_2$ compared to PbI_2. Some literature points towards the latter hypothesis, as the energetic stability of lead halides increases with increasing halide electronegativity (from iodide to bromide).[36,37]

The vacuum-deposited 2D perovskite films were further studied by mean of time-resolved microwave conductivity (TRMC). Fig. 4 shows the time-dependent photoconductivity traces for all the 2D perovskites reported here. Three different excitation wavelength (pulsed laser excitation at 510 nm, 403 nm and 445 nm) were applied according to the maximum absorption at the excitonic peak of each compound. Upon excitation, electron-hole pairs are generated within the inorganic sheets of the 2D perovskite and, due to the strong confinement (large E_b), they will mostly exist as bound excitons, hence not contributing to the photoconductance. This is important as in these compounds the TRMC signal is not directly a measure of the charge mobility, but rather its product with the free carrier generation yield.[14]

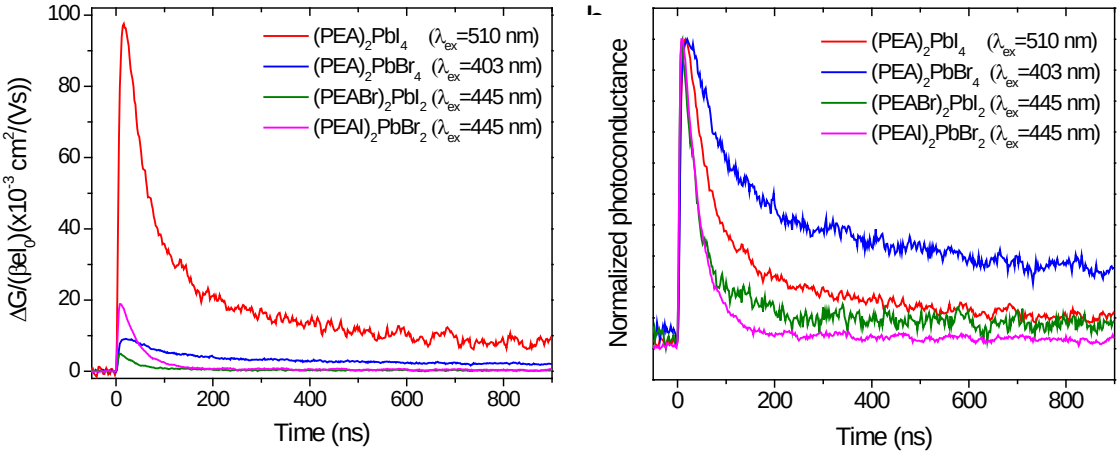

Fig. 4 (a) Time-resolved microwave conductivity traces of vacuum-deposited 2D perovskite selectively excited at 510, 403 and 445 nm. (b) normalize time-dependent photoconductance of the same sample series.

From the maximum change in TRMC signal (Fig. 4a), recorded with an excitation density on the order of 10^{12} photons/cm^2, one can immediately observe that the pure iodide 2D compound $(PEA)_2PbI_4$ present a larger photoconductance (0.1 cm^2/Vs) as compared to the bromide and mixed halide analogs. The photoconductance of $(PEA)_2PbI_4$ is consistent with the low yield of excitons dissociation into mobile carriers, and is comparable to previously reported values for similar solution-processed 2D perovskite films.[14] The lower absolute photoconductance observed for $(PEA)_2PbBr_4$ and mixed $(PEABr)_2PbI_2$ and $(PEAI)_2PbBr_2$ film can be ascribed to the lower crystal/grain size, as observed by electron microscopy (Fig. 2). Among these materials, the larger grains in $(PEAI)_2PbBr_2$ films might hence be responsible for the slightly higher photoconductance observed for this specific compound (0.02 cm^2/Vs). In order to evaluate the charge carrier recombination, the TRMC traces were normalized (Fig. 4b) allowing a direct comparison of the recombination lifetime $t_{1/2}$ (time after excitation when the charge carrier concentration drops to 1/2 of its initial value). Interestingly, the pure bromide $(PEA)_2PbBr_4$ perovskite showed a longer lifetime (160 ns) compared to the pure 2D iodide films ($t_{1/2}$ = 70 ns). This trend is somewhat unexpected, as E_b was reported to increase when moving from iodide to bromide perovskites, implying a lower photoconductance but also a lower lifetime for bromide compounds.[38] The larger

lifetime is hence most likely correlated with the presence of iodide in $(PEA)_2PbBr_4$, acting as carrier traps and causing slower charge recombination within the material. Finally, the overall lower lifetimes observed for the mixed compounds (40 ns) correlates with an increased disorder due to the presence of mixed halide domains. In all cases the lifetime values observed here well compare with literature data.[14]

In summary, we have presented the dual-source vacuum deposition of 2D perovskite films of the type PEA_2PbX_4, where PEA is phenetylammonium and X stands for I^-, Br^-, or a combination of both. As for vacuum-deposited 3D perovskite films, we observed a high degree of crystallinity for all 2D compounds even at room temperature, a remarkable feature which is advantageous for the fabrication of multilayer perovskite stacks. The 2D perovskite films exhibited the expected trend in bandgap, increasing from the pure iodide to pure bromide materials, and intermediate for the mixed halide compounds. Through the series of experiments carried out here, we have observed an unavoidable halide cross-contamination among different deposition runs. Its implication is particularly relevant for the fabrication of wide bandgap perovskite films (here $(PEA)_2PbBr_4$), where the presence of iodide unavoidably results in multiple luminescence features due to the heterogeneous energy landscape within the semiconductor. Hence it is mandatory to have a dedicated chamber for a given composition in order to ensure the formation of high purity perovskite compounds. We have also investigated the preparation of mixed I/Br 2D perovskites by co/sublimation of either PEAI and $PbBr_2$ or vice versa. Interestingly, Br/I 1:1 stoichiometry could only be obtained when using PbI_2 and PEABr, most likely due to the higher reactivity of PbI_2 (as compared to the more stable $PbBr_2$) towards the organic cations. This is another important observation to be considered when designing vacuum deposition of low-dimensional, mixed halide compounds. The materials were also analyzed by time-resolved microwave conductivity (TRMC). The pure iodide PEA_2PbX_4 showed photoconductance and lifetime values in agreement with previously reported solution-processed thin films, making it an interesting candidate for implementation in multilayer optoelectronic devices.

Conflicts of interest

There are no conflicts to declare.

Acknowledgements

The research leading to these results has received funding from the European Union Programme for Research and Innovation Horizon 2020 (2014–2020) under the Marie Skłodowska-Curie Grant Agreement PerovSAMs No. 747599 and the Spanish Ministry of Economy and Competitiveness (MINECO) via the Unidad de Excelencia María de Maeztu MDM-2015-0538, MAT2017-88821-R, PCIN-2015-255, PCIN-2017-014, and the Generalitat Valenciana (Prometeo/2016/135). M.S. acknowledges the MINECO for his RyC contract. D.G acknowledges the funding from the China Scholarship Council (CSC).

Notes and References

1 D. B. Mitzi, K. Chondroudis and C. R. Kagan, *IBM J. Res. Dev.*, 2001, **45**, 29–45.

2 A. Lemmerer and D. G. Billing, *CrystEngComm*, 2012, **14**, 1954.

3 M. D. Smith, B. A. Connor and H. I. Karunadasa, *Chem. Rev.*, 2019, **119**, 3104–3139.

4 M. Saliba, *Adv. Energy Mater.*, 2019, **9**, 1803754.

5 M. D. Smith, E. J. Crace, A. Jaffe and H. I. Karunadasa, *Annu. Rev. Mater. Res.*, 2018, **48**, 111–136.

6 S. Tao, I. Schmidt, G. Brocks, J. Jiang, I. Tranca, K. Meerholz and S. Olthof, *Nat. Commun.*, 2019, **10**, 2560.

7 C. Katan, N. Mercier and J. Even, *Chem. Rev.*, 2019, **119**, 3140–3192.

8 T. Ishihara, X. Hong, J. Ding and A. V. Nurmikko, *Surf. Sci.*, 1992, **267**, 323–326.

9 Hong, Ishihara and Nurmikko, *Phys. Rev. B. Condens. Matter*, 1992, **45**, 6961–6964.

10 G. Kieslich, S. Sun and A. K. Cheetham, *Chem. Sci.*, 2015, **6**, 3430–3433.

11 S. Ahmad, C. Hanmandlu, P. K. Kanaujia and G. V. Prakash, *Opt. Mater. Express*, 2014, **4**, 1313.

12 A. Raja, A. Chaves, J. Yu, G. Arefe, H. M. Hill, A. F. Rigosi, T. C. Berkelbach, P. Nagler, C. Schüller, T. Korn, C. Nuckolls, J. Hone, L. E. Brus, T. F. Heinz, D. R. Reichman and A. Chernikov, *Nat. Commun.*, 2017, **8**, 15251.

13 D. B. Straus and C. R. Kagan, *J. Phys. Chem. Lett.*, 2018, **9**, 1434–1447.

14 M. C. Gélvez-Rueda, E. M. Hutter, D. H. Cao, N. Renaud, C. C. Stoumpos, J. T. Hupp, T. J. Savenije, M. G. Kanatzidis and F. C. Grozema, *J. Phys. Chem. C*, 2017, **121**, 26566–26574.

15 M. Era, S. Morimoto, T. Tsutsui and S. Saito, *Appl. Phys. Lett.*, 1994, **65**, 676–678.

16 K. Chondroudis and D. B. Mitzi, *Chem. Mater.*, 1999, **11**, 3028–3030.

17 C. R. Kagan, D. B. Mitzi and C. D. Dimitrakopoulos, *Science (80-.).*, 1999, **286**, 945–947.

18 Y. Liu, H. Ye, Y. Zhang, K. Zhao, Z. Yang, Y. Yuan, H. Wu, G. Zhao, Z. Yang, J. Tang, Z. Xu and S. (Frank) Liu, *Matter*, 2019, **1**, 465–480.

19 Y. Zhang, Y. Liu, Z. Xu, H. Ye, Q. Li, M. Hu, Z. Yang and S. (Frank) Liu, *J. Mater. Chem. C*, 2019, **7**, 1584–1591.

20 I. C. Smith, E. T. Hoke, D. Solis-Ibarra, M. D. McGehee and H. I. Karunadasa, *Angew. Chemie*, 2014, **126**, 11414–11417.

21 G. Grancini, C. Roldán-Carmona, I. Zimmermann, E. Mosconi, X. Lee, D. Martineau, S. Narbey, F. Oswald, F. De Angelis, M. Graetzel and M. K. Nazeeruddin, *Nat. Commun.*, 2017, **8**, 15684.

22 X. Zhu, D. Yang, R. Yang, B. Yang, Z. Yang, X. Ren, J. Zhang, J. Niu, J. Feng and S. (Frank) Liu, *Nanoscale*, 2017, **9**, 12316–12323.

23 M. Era, T. Hattori, T. Taira and T. Tsutsui, *Chem. Mater.*, 1997, **9**, 8–10.

24 K. M. Chiang, B. W. Hsu, Y. A. Chang, L. Yang, W. L. Tsai and H. W. Lin, *ACS Appl. Mater. Interfaces*, 2017, **9**, 40516–40522.

25 D. B. Mitzi, M. T. Prikas and K. Chondroudis, *Chem. Mater.*, 1999, **11**, 542–544.

26 Z. Zheng, H. Lan, Z. Su, H. Peng and J. Luo, *Sci. Rep.*, 2019, 1–9.

27 J. Ávila, C. Momblona, P. P. Boix, M. Sessolo and H. J. Bolink, *Joule*, 2017, **1**, 431–442.

28 R. C. Shallcross, S. Olthof, K. Meerholz and N. R. Armstrong, *ACS Appl. Mater. Interfaces*, 2019, **11**, 32500–32508.

29 K. Du, Q. Tu, X. Zhang, Q. Han, J. Liu, S. Zauscher and D. B. Mitzi, *Inorg. Chem.*, 2017, **56**, 9291–9302.

30 D. B. Mitzi, *Synthesis, Structure, and Properties of Organic-Inorganic Perovskites and Related Materials*, 1994.

31 G. C. Papavassiliou, G. A. Mousdis, C. P. Raptopoulou and A. Terzis, *Zeitschrift für Naturforsch. B*, 1999, **54**, 1405–1409.

32 K. Shibuya, M. Koshimizu, F. Nishikido, H. Saito and S. Kishimoto, *Acta Crystallogr. Sect. E. Struct. Rep. Online*, 2009, **65**, m1323-4.

33 D. . Mitzi, *J. Solid State Chem.*, 1999, **145**, 694–704.

34 C. C. Stoumpos, D. H. Cao, D. J. Clark, J. Young, J. M. Rondinelli, J. I. Jang, J. T. Hupp and M. G. Kanatzidis, *Chem. Mater.*, 2016, **28**, 2852–2867.

35 G. Longo, C. Momblona, M.-G. La-Placa, L. Gil-Escrig, M. Sessolo and H. J. Bolink, *ACS Energy Lett.*, 2018, **3**, 214–219.

36 G. P. Nagabhushana, R. Shivaramaiah and A. Navrotsky, *Proc. Natl. Acad. Sci.*, 2016, **113**, 7717–7721.

37 I. L. Ivanov, A. S. Steparuk, M. S. Bolyachkina, D. S. Tsvetkov, A. P. Safronov and A. Y. Zuev, *J. Chem. Thermodyn.*, 2018, **116**, 253–258.

38 Y. Gao, M. Zhang, X. Zhang and G. Lu, *J. Phys. Chem. Lett.*, 2019, **10**, 3820–3827.

SUPPLEMENTARY INFORMATION

Dual-source vacuum deposition of pure and mixed halide 2D perovskites: thin film characterization and processing guidelines.

Maria-Grazia La-Placa,[a] Dengyang Guo,[b] Lidón Gil-Escrig,[c] Francisco Palazon,[a] Michele Sessolo,*[a] Henk J. Bolink[a]

[a] *Instituto de Ciencia Molecular, Universidad de Valencia, C/ Beltrán 2, Paterna, 46980, Spain. E-mail: michele.sessolo@uv.es*

[b] *Department of Chemical Engineering, Delft University of Technology, Delft, 2629 HZ, The Netherlands*

[c] *Helmholtz-Zentrum Berlin für Materialien und Energie GmbH, Young Investigator Group for Perovskite Tandem Solar Cells, Kekuléstraße 5, Berlin, 12489, Germany*

Experimental Section

Materials. $C_8H_{12}IN$ (PEAI) and $C_8H_{12}BrN$ (PEABr) were purchased from Lumtec. PbI_2 and $PbBr_2$ were purchased from Tokyo Chemical Industry CO (TCI). All materials were used as received.

Thin-films preparation. ITO-coated glass and glass substrates were subsequently cleaned with soap, water and isopropanol in an ultrasonic bath, followed by UV-ozone treatment. They were transferred to a vacuum chamber integrated into a nitrogen-filled glovebox (H_2O and O_2 < 0.1 ppm) and evacuated to a pressure of 10^{-6} mbar. The vacuum chamber used to sublimate the organic halides PEAI and PEABr and lead salts PbI_2 and $PbBr_2$ was equipped with temperature-controlled evaporation sources (Creaphys) fitted with ceramic crucibles and independent temperature controllers and shutters. Three quartz crystal microbalance (QCM) sensors were used: two monitoring the deposition rate of each evaporation source and a third one close to the substrate holder monitoring the total deposition rate. All the sources were individually calibrated for its respective material.

XRD characterization. X-ray diffractograms were collected with a Panalytical Empyrean diffractometer equipped with CuKα anode operated at 45 kV and 40 mA and a PIXcel 1D detector

in scanning line mode. Single scans were acquired in the 2Θ = 5° to 50° range, in Bragg-Brentano geometry in air. All XRD analysis was carried out with Fullprof software. Whole-pattern Le Bail fits assuming a Thompson-Cox-Hastings pseudo-Voigt lineshape are performed to refine lattice parameters.

Optical Characterization. Absorption spectra were collected using a fiber optics based Avantes Avaspec 2048 Spectrometer in air. Photoluminescence was measured using a compact fluorescence lifetime spectrometer C11367, Quantaurus- Tau, with continuous wave 340 nm LED light source, in air.

Morphological Characterization. The surface morphology of the thin films was analyzed using atomic force microscopy (AFM,Multimode SPM, Veeco, USA). Electron microscopy characterization (SEM and EDX) was performed using a Hitachi S-4800 microscope operating at an accelerating voltage of 10 kV.

Time-resolved microwave conductivity. For the TRMC measurements, the 2D perovskite films were mounted in a sealed microwave resonance cavity within a nitrogen glovebox. The TRMC technique monitors the change in reflected microwave power by the loaded microwave cavity upon pulsed laser excitation at various wavelengths (403 nm, 445 nm, and 510 nm). The photo-conductance (ΔG) of the sample was deduced from the laser-induced change in normalized microwave power (ΔP/P) by

$$-\mathrm{K}\Delta\mathrm{G}(\mathrm{t}) = \frac{\Delta\mathrm{P}(\mathrm{t})}{\mathrm{P}}$$

where K is the sensitivity factor. The yield of generated free charges φ and mobility $\sum\mu = (\mu_e + \mu_h)$ comprise the photoconductance, ΔG_{max}:

$$\eta\sum\mu = \frac{\Delta G_{max}}{I_0 e\beta}$$

Normalized TRMC traces can specifically show comparison of samples on charge carrier decay

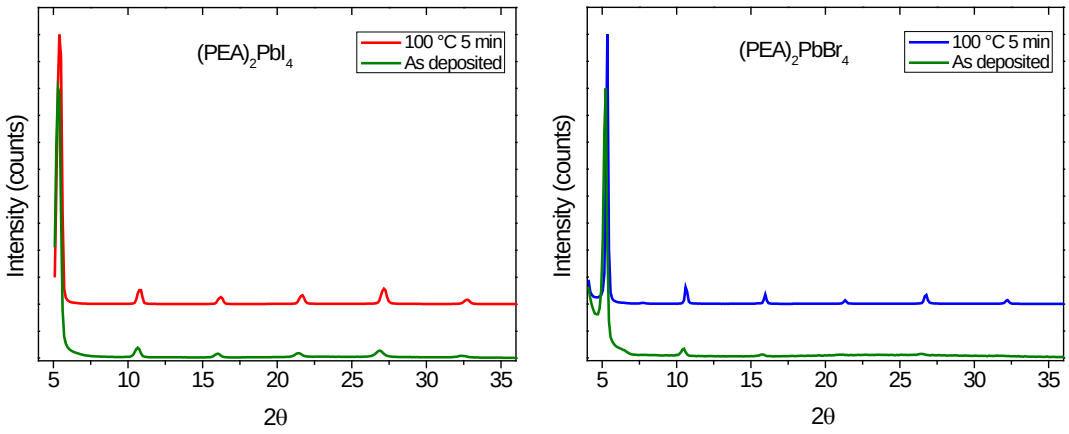

Figure S1. XRD patterns of a vacuum deposited a) PEA_2PbI_4 and b) PEA_2PbBr_4 measured as prepared

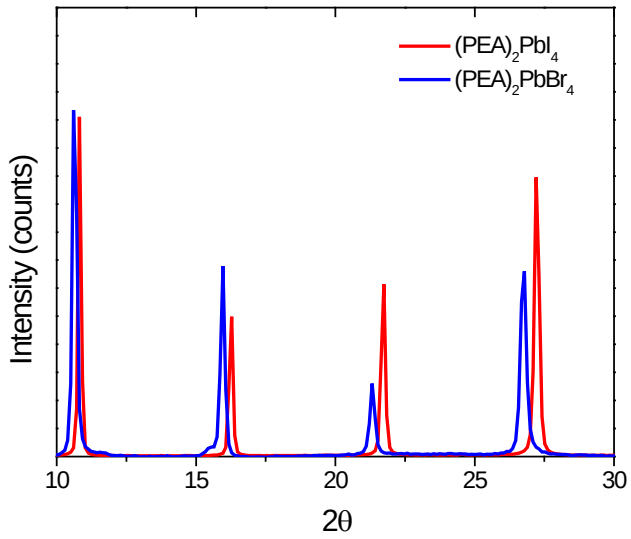

Figure S2. XRD patterns of a vacuum deposited PEA_2PbI_4 and PEA_2PbBr_4

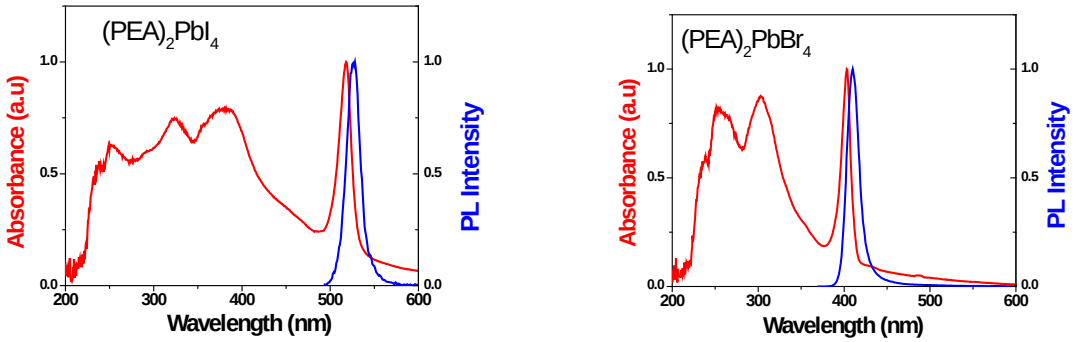

Figure S3. Optical absorption and photoluminescence of 2D PEA_2PbI_4 (λ_{abs} 518 nm, FWHM 20 nm and λ_{em} 528 nm, FWHM 19 nm) and 2D PEA_2PbBr_4 (λ_{abs} 403 nm, FWHM 14 nm and λ_{em} 410 nm, FWHM 17 nm) perovskites thin films prepared from solution process.

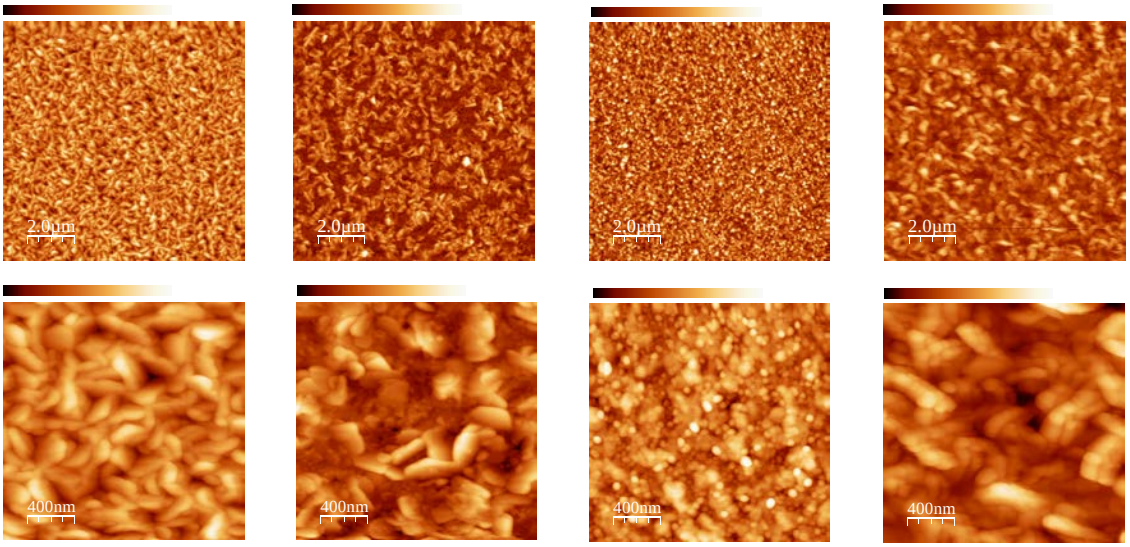

Figure S4. AFM topographies at different magnifications of a) PEA_2PbI_4, b) PEA_2PbBr_4 c) $(PEABr)_2PbI_2$ and d) $(PEAI)_2PbBr_2$ 2D perovskite thin films.

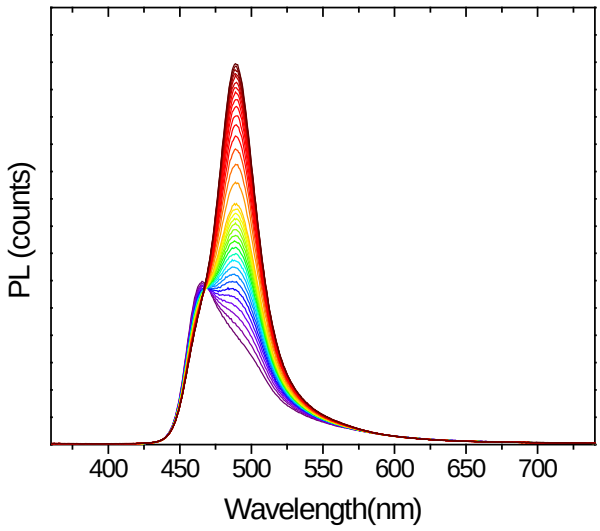

Figure S5. Evolution of the photoluminescence spectra of the $(PEABr)_2PbI_2$ thin film under continuous excitation with a CW laser at 375 nm. Each spectrum is collected every 10 s, going from purple to dark red.